Elsevier Editorial System(tm) for Physica Medica: European Journal of Medical Physics
Manuscript Draft

Manuscript Number:

Title: Design Optimization of a Pixel-Based Range Telescope for Proton Computed Tomography

Article Type: SI: Geant4 Advances

Keywords: proton computed tomography; detector optimization; monte carlo simulation; track reconstruction

Corresponding Author: Dr. Helge Egil Seime Pettersen, Ph.D.

Corresponding Author's Institution: Department of oncology and medical physics, Haukeland University Hospital

First Author: Helge Egil Seime Pettersen, Ph.D.

Order of Authors: Helge Egil Seime Pettersen, Ph.D.; Johan Alme, Ph.D.; Gergely G Barnaföldi, Ph.D.; Rene Barthel; Anthony van den Brink; Viljar N Eikeland, MSc; Alba García-Santos; Ola Grøttvik, MSc; Håvard Helstrup, Ph.D.; Kristin F Hetland, Ph.D.; Shruti Mehendale, Ph.D.; Ilker Meric, Ph.D.; Odd Harald Odland, Ph.D.; Gábor Papp, Ph.D.; Thomas Peitzmann, Ph.D.; Pierluigi Piersimoni, Ph.D.; Dieter Röhrich, Ph.D; Joao Seco, Ph.D.; Hesam Shafiee, MSc; Eivind V Skjæveland, MSc; Jarle R Sølie, MSc; Ganesh J Tambave, Ph.D.; Kjetil Ullaland, Ph.D.; Monika Varga-Kofarago; Lennart Volz, MSc; Boris Wagner, Ph.D.; Shiming Yang, Ph.D.

Abstract: Purpose: A pixel-based range telescope for tracking particles during proton imaging is currently under development. The detector applies layers of laterally stacked Monolithic Active Pixel Sensors with fast readout speeds. This study evaluates design alternatives on basis of the protons' range accuracy and the track reconstruction efficiency.

Method: Detector designs with different thicknesses of the energy-absorbing plates between each sensor layers are simulated using the GATE / Geant4 Monte Carlo software. Each of the incoming proton tracks are reconstructed, and a Bragg curve fitting procedure is applied for the calculation of each proton's range.

Results: Simulations show that setups with 4 mm and thinner absorber thicknesses of aluminum have a low range uncertainty compared to the physical range straggling, systematic errors below 0.3 mm water equivalent thickness and would be able to track more than ten million protons per second.

Conclusions: In order to both restrict the total number of layers and yield the required tracking and range resolution properties, a design recommendation is reached where the proposed range telescope applies 3.5 mm thick aluminum absorber slabs between each sensor layer.

Cover letter

December 20, 2018

Dear Editor of Physica Medica,
We are submitting a manuscript for the consideration of publication in Physica Medica, for the special issue «Advances in Geant4 applications in medicine». The manuscript is entitled «Design Optimization of a Pixel Based Range Telescope for Proton Computed Tomography». It has not been published elsewhere: except for as an earlier version in the first author's doctoral dissertation, located at: http://bora.uib.no/handle/1956/17757. It has not been submitted simultaneously for publication elsewhere.

I hope you will consider this study on the optimization of a detector for proton Computed Tomography. It is a Monte Carlo based study where the thickness and materials of the energy absorbers sandwiched between sensor layers in the range telescope are determined, the results of which are to be applied during the construction of a similar detector at our facility. Similar range telescopes are also under consideration for proton CT usage elsewhere, ensuring the relevance of this study.

Thank you for your consideration.

Sincerly,
Dr. Helge Egil Seime Pettersen
Haukeland University Hospital
Jonas Lies veg 65, 5021 Bergen
Norway
Email: helge.pettersen@helse-bergen.no

***Highlights (for review)**

- A pixel-based range telescope is a good candidate for proton computed tomography
- The detector design must be optimized for proton track reconstruction
- A design with 3.5 mm Al absorbers between the sensor layers is recommended
- Simulations show that particle rates of above ten million protons per second is possible

Design Optimization of a Pixel-Based Range Telescope for Proton Computed Tomography

Helge Egil Seime Pettersen[a,*], Johan Alme[b], Gergely Gábor Barnaföldi[c], Rene Barthel[d], Anthony van den Brink[d], Viljar Eikeland[b], Alba García-Santos[d], Ola Grøttvik[b], Håvard Helstrup[e], Kristin Fanebust Hetland[e], Shruti Mehendale[b], Ilker Meric[e], Odd Harald Odland[a], Gábor Papp[f], Thomas Peitzmann[d], Pierluigi Piersimoni[b], Dieter Röhrich[b], Joao Seco[g,h], Hesam Shafiee[b,e], Eivind Vågslid Skjæveland[e], Jarle Rambo Sølie[b,e], Ganesh Tambave[b], Kjetil Ullaland[b], Monika Varga-Kofarago[c], Lennart Volz[g,h], Boris Wagner[b], Shiming Yang[b]

[a] *Department of Oncology and Medical Physics, Haukeland University Hospital, 5021 Bergen, Norway*
[b] *Department of Physics and Technology, University of Bergen, 5007 Bergen, Norway*
[c] *Wigner Research Center for Physics, 1121 Budapest, Hungary*
[d] *Institute for Subatomic Physics, Utrecht University/Nikhef, Utrecht, Netherlands*
[e] *Department of Electrical Engineering, Western Norway University of Applied Science, 5063 Bergen, Norway*
[f] *Institute for Physics, Eötvös Loránd University, 1/A Pázmány P. Sétány, H-1117, Budapest, Hungary*
[g] *Department of Biomedical Physics in Radiation Oncology, German Cancer Research Center, Heidelberg, Germany*
[h] *Department of Physics and Astronomy, Heidelberg University, Heidelberg, Germany*

Abstract

Purpose: A pixel-based range telescope for tracking particles during proton imaging is currently under development. The detector applies layers of laterally stacked Monolithic Active Pixel Sensors with fast readout speeds. This study evaluates design alternatives on basis of the protons' range accuracy and the track reconstruction efficiency.
Method: Detector designs with different thicknesses of the energy-absorbing plates between each sensor layer are simulated using the GATE / Geant4 Monte Carlo software. The incoming proton tracks are individually reconstructed, and a Bragg curve fitting procedure is applied for the calculation of each proton's range.
Results: Simulations show that the setups with 4 mm and thinner absorber layers of aluminum have a low range uncertainty compared to the physical range straggling, systematic errors below 0.3 mm water equivalent thickness and would be able to track more than ten million protons per second.
Conclusions: In order to both restrict the total number of layers and yield the required tracking and range resolution properties, a design recommendation is reached where the proposed range telescope applies 3.5 mm thick aluminum absorber slabs between each sensor layer.

Keywords: Proton Computed Tomography, Detector Optimization, Monte Carlo Simulation, Track Reconstruction

1. INTRODUCTION

Proton Computed Tomography (proton CT) is an imaging modality enabling the measurement of the proton stopping power in the patient: prior to treatment planning and treatment in proton therapy [1], with the target of increasing the accuracy of the proton range estimation compared to conversion from

*Corresponding author
Email address: helge.pettersen@helse-bergen.no (Helge Egil Seime Pettersen)

the X-ray mass attenuation [2]. Several design approaches for proton CT have been proposed. Usually, tracker planes in front of and behind the patient measure each proton's position and direction so that its path through the patient can be estimated [3, 4]. The residual range or energy of each proton is then measured using range telescopes or scintillator calorimeters. Position-sensitive range telescopes have been proposed in Pettersen *et al.* [5] with pixel detectors and in Esposito *et al.* [6] with silicon strip detectors: these systems are able to measure a high number of protons in a single readout cycle, thereby increasing the proton intensity capacity.

The aim for this study is to optimize the various properties of the design of a pixel-based range telescope for proton CT. The simultaneous optimization of the following metrics is performed: accuracy and precision of the range determination; high track reconstruction efficiency, *i.e.* the ability to disentangle and reconstruct all incident protons in a single readout frame; and other constraints such as cost (the number of layers), cooling and mechanical stability. We apply the experience from a proof-of-concept detector [5] in order to propose a design for the next prototype.

The range accuracy will have impact on the degree to which the proton stopping power map of the patient's body can be correctly calculated. A low range uncertainty and an efficient track reconstruction enables that fewer protons are needed during the scan, *i.e.* a lower dose to the patient and a shorter scan time and a higher signal to noise ratio.

The design optimization is here performed through the determination of an optimized thickness of the energy absorber material between the sensor layers, as well as the choice of the absorber material. Several different values for the thicknesses are evaluated by means of Monte Carlo (MC) simulations, using the GATE 7.2 / Geant4 9.6.4 software [7, 8].

1.1. The ALPIDE Pixel Chip

The sensor chip for the range telescope is the ALice PIxel DEtector (ALPIDE) chip [9], which is a Monolithic Active Pixel Sensor (MAPS) with 1-bit digital "hit-or-no-hit" readout based on a pre-set threshold. The planned upgrade of the ALICE Inner Tracking System (ITS) is based on the ALPIDE chip, which has been developed for that specific purpose [10]. Each chip has an active area of approximately $3 \times 1.5\,\mathrm{cm}^2$: from a 1024×512 pixel array of $28 \times 28\,\mu\mathrm{m}^2$ pixels. The chip has a fast programmable integration time of ~5–10 µs, with a readout chain capable of handling a continuous readout at that rate: it is achieved by the reduction of data, through the regional pixel readout via a priority encoder, a multi-event memory and a *zero-suppression* technique where only activated pixels send a signal. More details on the integration of the ALPIDE chips into the proton CT system can be found in Grøttvik [11].

Since the ALPIDE chips have a 1-bit digital readout per pixel, it is not possible to directly measure the energy deposited in each pixel. However, Maczewski [12] and Pettersen [13] propose models for determining the energy deposited by means of counting the number of activated pixels in the area surrounding a proton track. These models, when adapted to the ALPIDE chips, are expected to aid in the reconstruction of proton tracks and the filtering of secondary particles (if the energy deposition signatures of the particles are sufficiently separated for cluster size discrimination). For the sake of simplicity, and due to that ALPIDE's energy deposition–cluster size relationship is not sufficiently explored in the context of <250 MeV protons, in this study we directly apply the deposited energy as read out from the MC software for the purposes of track reconstruction.

2. DETECTOR DESIGN GUIDELINES

The proton CT system is to be built by stacking 25–70 large-area arrays of pixel sensor layers longitudinally, the sensor layers being interleaved with energy-absorbing layers. Several geometrical configurations are needed in order to compare and evaluate the desired detector metrics. It is possible to define a large number of potential designs for the detector, and therefore some constraints must be put on the degrees of freedom in this work. A baseline design based on the original prototype from Pettersen *et al.*

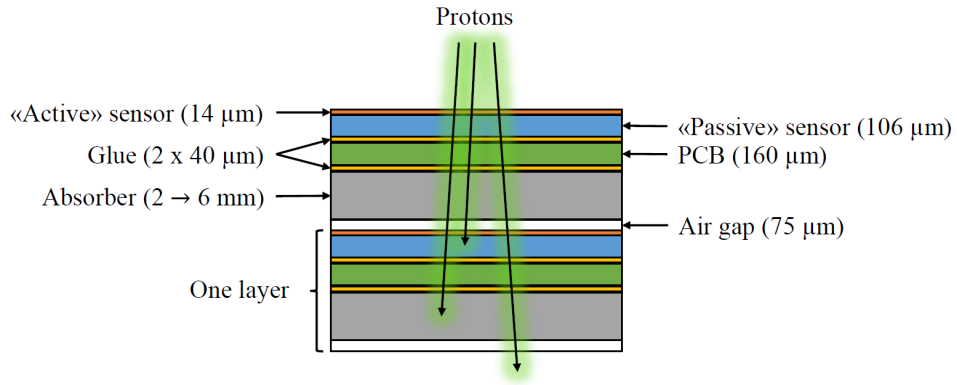

Figure 1: The design to be optimized: Different thicknesses (2–6 mm) for the energy absorbers are considered, and evaluated through the MC simulations. To fully slow down and stop a 230 MeV proton, 25–70 layers are needed. Only the "active" sensor volumes are used as sensitive volumes in the MC simulations [13].

[5] is shown in Figure 1. While the geometry of the sensor chips and electronic components are unaltered, the energy absorbers between the sensor layers are chosen to be between 2 mm and 6 mm aluminum. The material choice is discussed in the following.

In order to achieve a high accuracy in the measurement of the initial proton vectors, the two first sensor-absorber layers should contain as little mass as possible [14]. To this end, the first absorber layer is removed and to be replaced with a low-mass stabilizer.

Details such as chip bonding, aspects related to the mechanical structure, heat sink design and the readout electronics are out of scope of this work and, also, not yet finally decided upon. As a result of this, the exact results of the simulations will not reflect the detailed final prototype. Several simplifications are made during the geometrical designs for the MC simulations, such as using homogeneous slabs of materials rather than implementing accurate designs with details such as the ALPIDE chips bonded to the PCB, glued to a backing together with absorbers and heat sinks, all mounted to a scaffolding. Nevertheless, the longitudinal distribution of materials will be modeled and included to the level of available knowledge.

2.1. The Absorber Material

Different materials are available as the absorber material. Material properties such as proton stopping- and scattering power, durability, ease of machining and mounting, thermal conductivity, thermal expansion of the absorber material and secondary neutron production must be considered, as well as the interface between the absorber and the aluminum carrier board for the sensor chips (*e.g.* having similar thermal expansion coefficients). See Table 1 for a list of different properties: the water equivalent thickness (WET) is found by finding the thickness which yields the same stopping power as 4 mm water. The angular dispersion in a thin layer due to MCS can be calculated using the Rossi-Greisen equation [15]:

$$\sigma_{\mathrm{MCS}} = \frac{21.1}{\sqrt{2}} \frac{1}{\beta p} \sqrt{\frac{x}{X_0}} \simeq 0.1 \sqrt{\frac{x}{X_0}}, \tag{1}$$

where βp are the kinematic variables for momentum and velocity, X_0 is the radiation length and x is the layer thickness and the last approximation holds for the energies of interest [16]. The scattering angle is calculated using Equation (1) for a therapeutic proton through a 4 mm WET slab. The neutron yield is the number of neutrons produced per incoming proton (150 MeV beam in a slab of 4 mm WET, found in the GATE simulations by using the `QGSP_BIC_HP` physics builder list and 10^5 primaries).

Material	PMMA	Carbon Fiber	Aluminum	Copper	Tungsten
4 mm WET [mm]	3.46	2.24	1.9	0.66	0.4
4 mm WET scattering angle [mrad]	9.0	10.9	14.6	21.4	33.8
4 mm WET neutron yield [10^{-4}]	69.2	71.9	80.9	74.1	26.9
Thermal conductivity [W/mK]	0.25	800	205	401	174
Thermal expansion [10^{-6} K^{-1}]	70	2–4	21–24	16	4.5

Table 1: Properties of the potential absorber materials [19, 20, 21, 13, 22]. The scattering angle is calculated using Equation (1).

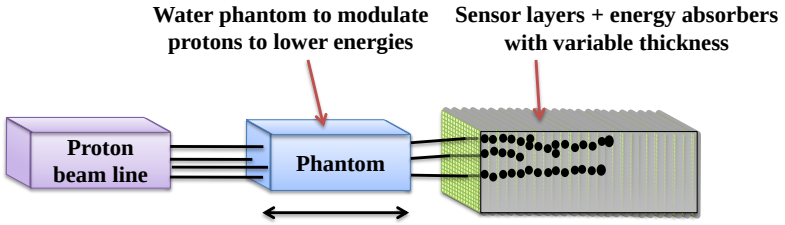

Figure 2: Schematic setup of the range calculation geometry. In order to obtain proton beams of different energy spectra from a 250 MeV beam, the thickness of the energy degrading water phantom is modulated from 0 cm to the maximum range of a 250 MeV beam, which corresponds to a water phantom length of approximately 38 cm [13].

Based on these, and in particular that the flexible PCB cables connected to the ALPIDE sensors are mounted to an aluminum backing, and when considering the ease of machining, the material of choice for the absorber is aluminum.

In terms of the stabilization of the first tracker layers, carbon fiber seems like a natural choice due to its thermal properties and low mass. Carbon fiber stabilization is also being explored in the context of the ALPIDE sensors in the ALICE-ITS upgrade [10, 17] for the ALICE experiment at the CERN LHC [18]. In Section 6.4 the effect on the proton trajectory estimation error of the scattering in the first layer material is calculated.

3. MONTE CARLO SIMULATIONS

To perform the data analysis to the level required to calculate the desired performance metrics, the MC simulations must contain the following: a proton beam with realistic spatial and (adjustable) spectral characteristics, and a sufficiently accurate geometrical implementation of a stack of the ALPIDE chips fixed to absorber layers of adjustable thicknesses.

A water phantom of variable thickness is used to slow down a 250 MeV proton beam, in order to represent realistic energy spectra with residual proton ranges that span the complete detector in depth. The water phantom thicknesses vary from zero to the maximum water equivalent range of the beam, approximately 38 cm, in steps of 1 mm to characterize the linearity of the range determination accuracy. The setup is shown in Figure 2. The stochastic energy loss throughout the phantom ensures that the resulting energy and spatial distribution of the proton beam incident on the detector is sufficiently realistic. The beam is generated as a pencil beam with a spot size of 3 mm placed 10 cm in front of the energy degrading water phantom. Its divergence is 2 mrad, and the emittance is 15 mm mrad.

The simulations have been performed using GATE 7.2 [7] together with Geant4 9.6.4 [8]. The physics builder list `QGSP_BIC_EMY` is used as suggested by Grevillot *et al.* [23], adjusted with a mean ionization potential for water of 75 eV in order to apply the PSTAR database [24] to calculate and compare the energy loss of the protons through the energy modulating water phantom.

The simulations have been carried out using 10^5 primary protons for each water phantom thickness, for each of the aluminum absorber thickness designs. This number represents a balance between the

total CPU requirements (5 geometries × 360 energies × 10^5 primaries) and the statistical quality of the distributions to be fitted (see Figure 4).

3.1. Proton Range from "MC Truth"

In the "MC truth" simulations, the complete detector geometry (including the aluminum absorbers) is setup as sensitive volumes, this to achieve a high accuracy of the residual proton ranges. In this case, for computational requirements, the number of primaries was reduced to 15 000 per 1 mm step size of the water phantom degrader thickness, per absorber thickness. A look-up-table containing phantom thicknesses, proton energies incident on the detector and residual ranges is created, to be retrieved using a cubic spline interpolation. This approach has been shown to yield high range accuracy [25]. This procedure is repeated for all design variants and water phantom thicknesses.

4. TRACK RECONSTRUCTION

One of the strengths of the pixel-based detector design is the ability to disentangle and reconstruct a large number of concurrent traversing proton tracks. To this end, a track reconstruction method has been developed, detailed in Pettersen *et al.* [26]. As an improvement to that algorithm, here we start the reconstruction process by choosing seeds from the distal end of the detector, such that the depths of both the starting and stopping position of each proton are known prior to reconstruction: this is, respectively, the first sensor layer and the distal sensor layer where the seed is located.

To summarize the tracking algorithm described in Pettersen *et al.* [26], a seed is chosen from the last traversed detector layer. Track candidates are grown towards the detector front face, each track segment chosen to minimize the distance between the extrapolated position and actual position of the candidate hit in the next layer. A track weight $S_n = \sqrt{\sum_{\text{layer}}^{n} (\Delta\theta_{\text{layer}})^2}$ is calculated, based on the accumulated angular change throughout the track, up to layer n. If $S_n > S_{\max}$ the track (segment) is discarded. If several track segment candidates are available, the best two are kept if they are sufficiently similar.[1] The actual value of $S_{\max}$ is chosen based on the expected scattering in the detector and on the track density (high track densities require a smaller $S_{\max}$ in order to avoid confusion). The procedure to find the optimal $S_{\max}$ value is based on a parameter scan of different $S_{\max}$ values applied on the track reconstruction of pencil beams—in Pettersen *et al.* [26] values of 150–300 mrad are identified, depending on the particle density.

After the reconstruction process, a few filters on the resulting tracks are applied. To remove tracks from non-multiple Coulomb scattering processes in the phantom, 3σ filters on the incoming angles and residual ranges are used [1]. In addition, a filter is put on the deposited energy in the last traversed layer in order to remove tracks undergoing inelastic collisions in the detector, and tracks that are incompletely reconstructed [13].

4.1. The Correctly Reconstructed Track

In order to benchmark the precision and efficiency of the track reconstruction algorithm, a definition of a correctly reconstructed track must be made: the first and last entry in a track must originate from the same proton history (identified by the `eventID` tag in GATE) and the last traversed (stopping) layer must be included in the reconstructed track. By following this definition, tracks have the correct incoming vector and the correct residual range, which are the required values for volumetric reconstruction of the stopping power map for proton CT purposes.

The *efficiency* of the track reconstruction is defined to be the ratio of correctly reconstructed tracks to the total number of tracks surviving the applied data filters.

[1] Both are kept if the next-to-best candidate's S_n value is at most 15% higher. Otherwise, only the best is kept. This procedure has been implemented in order to avoid an exploding number of track candidate splittings (one per layer).

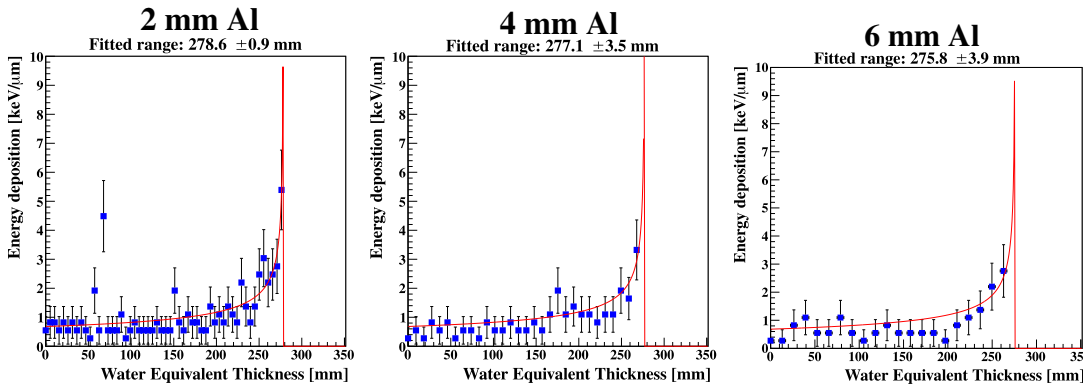

Figure 3: The deposited energies of individual proton tracks (in three different geometries), overlaid with a Bragg curve fit. The displayed "±" accuracy is the output from the least-squares method applied on an individual proton, and it is not representative for a proton beam of that energy. MC data taken with a 250 MeV beam degraded using a 10 cm water phantom. Some of the hits have a significantly higher deposited energy—these values can be explained by the Landau distributed energy loss process [13].

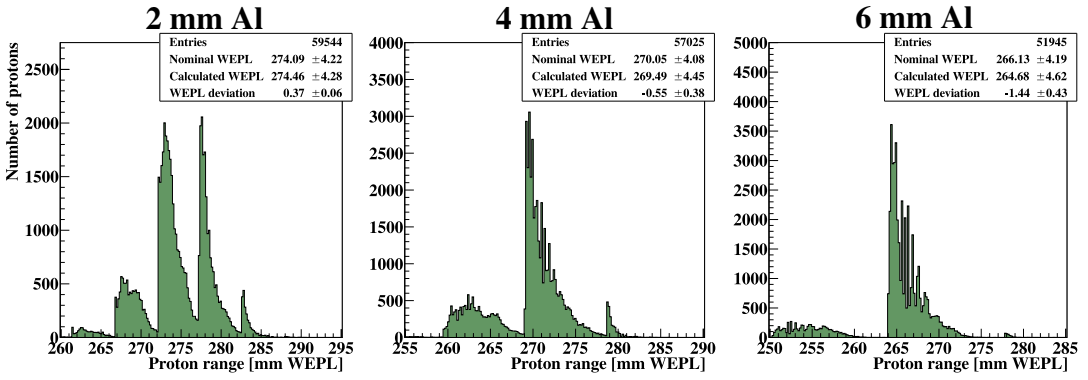

Figure 4: Distribution of the individual estimated ranges. From this distribution the residual range $\langle \hat{R} \rangle$ and range straggling $\langle \hat{\sigma}_R \rangle$ of a proton beam is calculated, shown in the text box as "$\langle \hat{R} \rangle \pm \langle \hat{\sigma}_R \rangle$". The characteristic pattern of the distribution, with regular sudden rises, can be seen in the figure. Each rise in the distribution is in coincidence with the beam reaching a new sensor layer. MC data taken with a 250 MeV monoenergetic proton beam degraded using a 10 cm water phantom [13].

5. RANGE CALCULATION

In order to obtain the best possible estimate of the performance of the different designs, the different parts of the analysis are treated separately: The track reconstruction step is omitted during the evaluation of the residual range calculation, where the tracks are obtained directly from the "MC truth" using the primary proton identification ID from GATE.

Using a perfect track reconstruction, the Bragg curve fitting methodology as described in Pettersen *et al.* [5] and below is applied to find the reconstructed range $\hat{R}$ of a single proton. The mean range $\langle\hat{R}\rangle$ and the corresponding mean range uncertainty $\langle\hat{\sigma}_R\rangle$ are found for each beam energy using Equation (3). It is also of interest to find any fluctuation of the range accuracy relative to the proton range relative to the sensor layer depth.

5.1. Range Calculation

While direct measurement of the energy loss is not possible using the proposed digital sensor readout (hit or no hit), it is possible to estimate the energy loss by counting the number of connected hits originating from the proton path, as described in detail in Pettersen *et al.* [5].

The pristine Bragg curve of a single proton's energy loss can be characterized using the "MC truth" range R and depth z together with the differentiated Bragg-Kleeman equation of Bortfeld [27]:

$$-\frac{\mathrm{d}E}{\mathrm{d}z} = \frac{p\alpha^{1/p}}{(R-z)^{1/p-1}}, \tag{2}$$

where p and α are model parameters fitted to the "MC truth" range-energy data. For the 4 mm aluminum absorber geometry, the parameters are $\alpha = 0.0211, p = 1.639$. This model was shown to yield a high accuracy in Pettersen *et al.* [25].

Least-squares fits of the reconstructed track's energy loss in each sensor layer to Equation (2) is performed to obtain $\hat{R}$. Examples from different geometries are shown in Figure 3. Note that the $\hat{R}$ values found using thinner absorber designs yields a higher range determination accuracy of individual proton tracks ($\hat{\sigma}_R$).

The "MC truth" range distribution of protons at the same initial energy is approximately Gaussian. However, the range distribution originating from the Bragg curve fitting is not Gaussian, and it is not trivial to describe the variations analytically due to the nature of the sparse measurements from each sensor layer: see Figure 4. However, a simple histogram calculation of the empirical mean value and standard deviation yields accurate results for the residual range $\langle\hat{R}\rangle$ and range uncertainty $\langle\hat{\sigma}_R\rangle$, respectively. The ranges of all protons in a beam (or in a voxel bin when performing the image reconstruction) contribute to a histogram with bin values z_i and bin heights w_i. The lower and upper limits for the range distribution z_1 and z_2, respectively, are defined as the $\mu \mp 4\sigma$ values of an initial Gaussian fit. Then, we have

$$\langle\hat{R}\rangle = \frac{\sum_{i=z_1}^{z_2} w_i z_i}{\sum_{i=z_1}^{z_2} w_i}, \qquad \langle\hat{\sigma}_R\rangle = \sqrt{\frac{\sum_{i=z_1}^{z_2} w_i (z_i - \langle\hat{R}\rangle)^2}{\left[\sum_{i=z_1}^{z_2} w_i\right] - 1}} \tag{3}$$

The above procedure is similar to the analysis of the proof-of-concept prototype [5], with the difference being the method of initially fitting the Gaussian distributions to the histogram values. In the geometries described here, a higher number of sensor layers are contained within a range distribution, and a higher accuracy of $\langle\hat{R}\rangle$ is expected.

5.2. Range Accuracy and Range Uncertainty

The range accuracy and range uncertainty resulting from a specific absorber design can be found by comparing the mean "MC truth" proton range R to the mean of the reconstructed proton range distribution

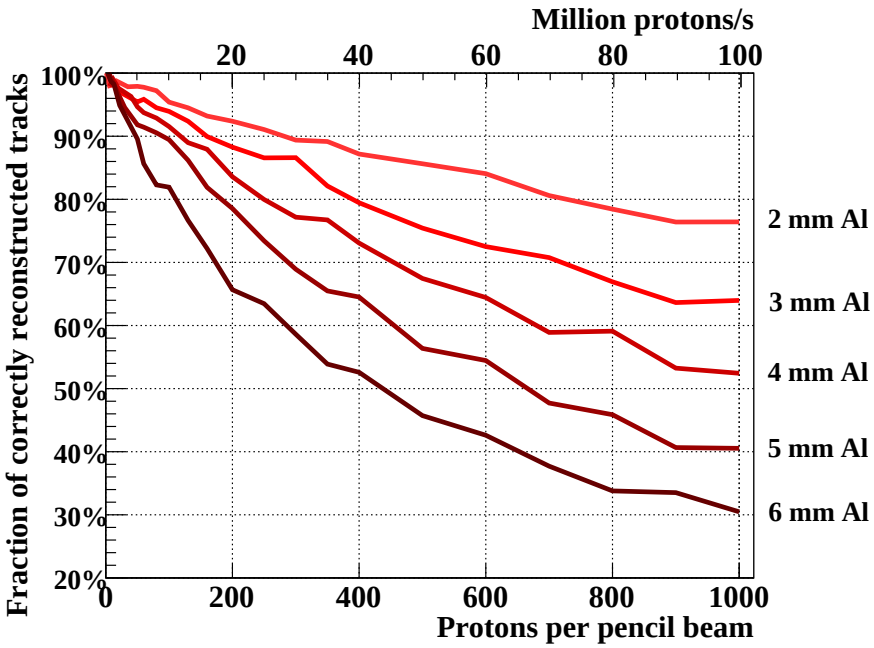

Figure 5: The fraction of correctly reconstructed tracks, as a function of the particle density, in the different geometries. The definitions of a correctly reconstructed track is given in Section 4.1, and an integration time of 10 µs is assumed.

$\langle \hat{R} \rangle$. The range accuracy, $\langle \langle \hat{R} \rangle - R \rangle$, is found by comparing the systematic error of the mean value of the range distribution throughout the full dynamic range of the detector (in terms of proton range). The range uncertainty is found by comparing the widths of the two distributions, respectively, σ_R and $\langle \hat{\sigma}_R \rangle$. Any additional width of the reconstructed range distribution is due to the degrading effects of the sparse sampling and to the analysis routine.

Since the range uncertainty due to range straggling is known from theory [27] and from the MC simulations, the intrinsic range uncertainty from the analysis can be calculated by subtracting in quadrature the expected range straggling from the measured range uncertainty.

It is not expected that the uncertainty and accuracy for a given geometry are the same at different incident proton energies, as the values are dependent on the relative position between the proton range position versus the sensor layer position: This effect was clearly seen in Pettersen *et al.* [5] where the absorbers consisted of 4.3 mm tungsten (having the same water equivalent thickness as 20.4 mm aluminum at 150 MeV).

6. RESULTS

6.1. Efficiency of the Track Reconstruction

The efficiency of the track reconstruction, as defined in Section 4.1, is shown in Figure 5 for the different designs under consideration. Is has been calculated by performing the track reconstruction 100 times with n_p concurrent protons, and finding the resulting percentage of correctly reconstructed tracks (see Section 4.1 for definition of a correctly reconstructed track). Then, the number of concurrent protons is varied from $n_p = 1$ to $n_p = 1000$ in order to evaluate the technique at different pencil beam intensities.

In the 4 mm design, a 90% efficiency is achieved with a pencil beam intensity of 118 protons per readout frame (11.8 million protons per second with 10 µs integration time), and a 80% efficiency is

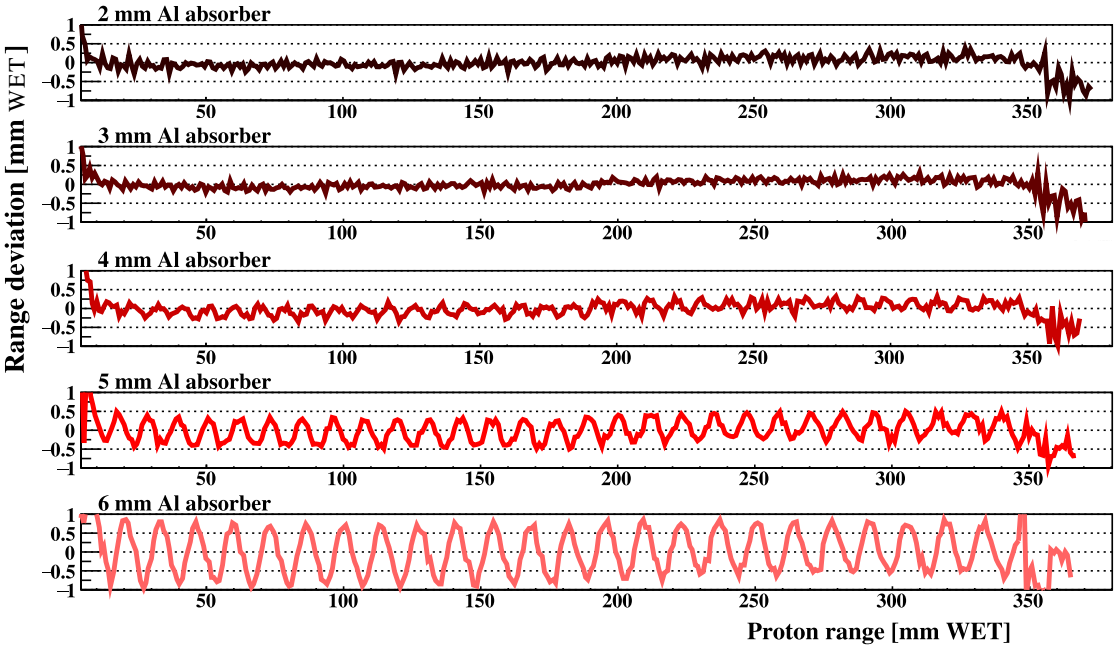

Figure 6: The range determination accuracy shown as the deviation between the "MC truth" range, and the reconstructed range $\langle \hat{R} \rangle$. For visualization purposes, a calibration constant of ~1 mm has been added to all ranges within a given geometry in the figure [13].

achieved with a similar intensity of 250 protons per readout frame (25 million protons per second): the proton rate at a certain efficiency increase approximately linearly with the area of the pencil beam.

Of the results presented in this study, the track reconstruction efficiency is the one that is most dependent on improvements of the algorithm. Further optimization of the track reconstruction algorithm will ensure that the reconstruction can be performed at higher beam intensities at high efficiencies.

6.2. Accuracy of the Range Calculation

The range accuracy is the systematic bias on the calculated proton range, found from the reconstructed ranges $\langle \hat{R} \rangle$ and the nominal ranges R through the relation $\langle \langle \hat{R} \rangle - R \rangle$ for each of the incident proton energies. In Figure 6 the range accuracy is shown for increasing incident energies in the different designs: The systematic errors are kept within 0.5 mm WET throughout the detector, for the designs having a 5 mm aluminum absorber or less. Note that a calibration constant in the order of 1 mm has been added to all ranges within a given geometry in the figure.

The dynamic range of the range telescope, given by the region with uniform range uncertainty and uniform range accuracy, is between 10 mm WET and 350 mm WET in the detector, or in terms of proton energy, between 35 MeV and 240 MeV. See Table 2 for the correspondence between the energies and the required number of layers.

6.2.1. Oscillating Error in the Range Accuracy

There is an oscillation artifact in the range accuracy. It is especially pronounced for the designs with 4 mm and thicker absorbers, and in the 2 mm and 3 mm designs it is negligibly small. The artifact is characterized by a sinusoidal shaped perturbation of the range accuracy.

The origin of the artifact is that the range straggling distribution of a proton beam spans several sensor layers (see Figure 4). The range accuracy depends on the number of sensor layers covered, and on the position of the mean value of the range distribution relative to the position of the adjacent sensor

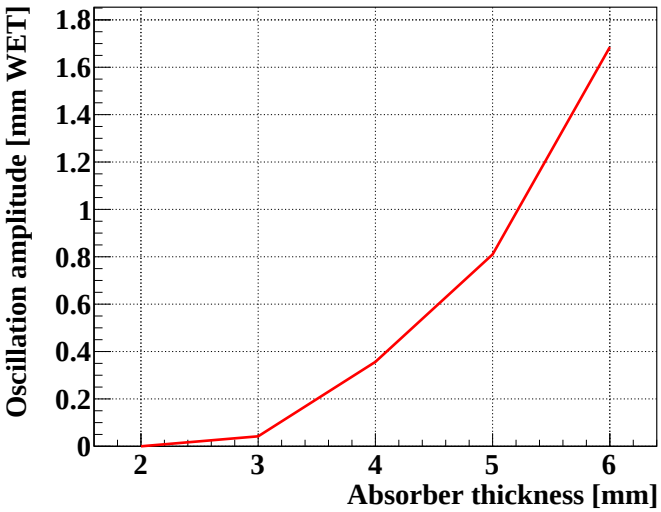

Figure 7: Measurements of the Fourier amplitude of the depth-dependent oscillation of the systematic range uncertainty [13].

layers. The more sensor layers that are covered by the range straggling distribution (*e.g.* thinner energy absorbers), the smaller the oscillation artifact. This was also seen in the proof-of-concept prototype detector [5], where range distributions that spanned two sensor layers had a significantly higher range accuracy compared to range distributions that only span a single sensor layer.

A quantitative measurement of the effect can be performed through a spectral analysis of the range accuracy distributions of Figure 6. The heights of the peaks in the Fourier spectra are measured, and these are compared to the amplitude measurements. While the Fourier spectra are more sensitive to small oscillation amplitudes, the peak heights need to be normalized to the oscillation amplitude.

In general the amplitudes of the oscillation are below 0.5 mm WET if the absorber is thinner than 4.5 mm aluminum, and below 0.2 mm WET for the 3.5 mm aluminum absorber geometry: see Figure 7 for the relationship between the absorber thickness and the oscillation amplitude.

6.2.2. Uncertainty of the Range Calculation

The uncertainty of the range calculation is calculated as the standard deviation of the fitted range distribution, $\langle\hat{\sigma}_R\rangle$. It is highly dependent on its lower physical limit, which is the statistical range straggling of the proton beam in the detector.

The mean measured range uncertainty $\langle\hat{\sigma}_R\rangle$ varies from 4.15 mm WET measured in the 2 mm aluminum absorber geometry, to 4.8 mm WET measured in the 6 mm aluminum absorber geometry. This is the expected overall uncertainty of the system. However, we need to consider that only a fraction of this number actually is due to the properties of the reconstruction process. The range straggling as predicted during the MC simulations where interactions in all volumes has been stored (σ_R) varies from 3.9 mm WET in the 2 mm aluminum absorber geometry to 3.8 mm WET in the 6 mm aluminum absorber geometry.[2]

Three curves are shown in Figure 8: the straggling as expected from a 250 MeV beam stopping in pure water, the "MC truth" straggling σ_R calculated from the simulations where the interactions from the full geometry has been stored and the measured uncertainty $\langle\hat{\sigma}_R\rangle$. Due to the heterogeneity of the

[2]The increased fraction of aluminum relative to the copper contents in the PCB reduces the straggling in the thicker absorber geometries.

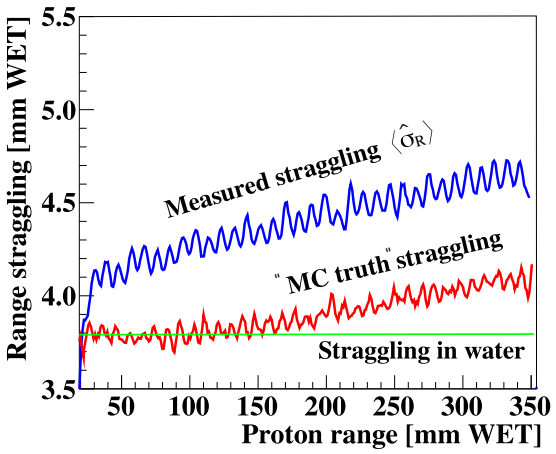

Figure 8: The measured range straggling $\langle\hat{\sigma}_R\rangle$, together with the actual straggling and the baseline straggling in water, for the 4 mm aluminum absorber geometry [13].

Absorber thickness [mm]	2	2.5	3	3.5	4	4.5	5	5.5	6
Layers needed (230 MeV)	66.6	55.2	47.1	41.1	36.5	32.8	29.7	27.2	24.4
Layers needed (200 MeV)	52.8	43.8	37.4	32.6	29	26	23.6	21.6	20

Table 2: The number of layers needed to contain a proton beam of 200 MeV and 230 MeV, in the different geometries, when a necessary extra margin corresponding to a distance of three times the range straggling is added [13].

detector, we expect the (water equivalent) range straggling in the detector to be above that of water and this is observed.

The added *intrinsic* uncertainty of the reconstruction process and simulation of the detector can be calculated as the subtraction between the two in quadrature:

$$\sigma_{R,\text{Intrinsic}} = \sqrt{\langle\hat{\sigma}_R\rangle^2 - \sigma_R^2} \tag{4}$$

The values for the average intrinsic uncertainty are 1.4 mm WET in the 2 mm aluminum absorber geometry; 2.15 mm WET in the 4 mm aluminum absorber geometry; and 2.9 mm WET in the 6 mm aluminum absorber geometry. These values are shown in Figure 9 for the different designs.

6.3. Required Number of Sensor Layers

The number of layers required to contain the complete proton beam has been found for the different designs studied here. Two monoenergetic proton beams are applied here: 200 MeV and 230 MeV. The necessary dynamic range is defined as the range plus 3 times the range straggling (to accurately measure the tails of the beam): this leads to the required number of layers, listed in Table 2.

6.4. Impact on the Tracking Resolution In Patient due to Scattering

One of the required measurements during the proton CT image acquisition is that of the direction of the incoming proton, by using measurements from the first two sensor layers. Any material in the first two sensor layers (*i.e.* the sensor chips, the flexible PCB and the carrier backing material) will scatter the incoming protons. The angular dispersion is calculated using the Rossi-Greisen equation of Equation (1).

Carbon fiber (CF), such as the Mitsubishi DIALED K13D2U [22] under consideration for the ALICE Inner Tracking System upgrade [10], has been proposed as a carrier backing material in the low-mass

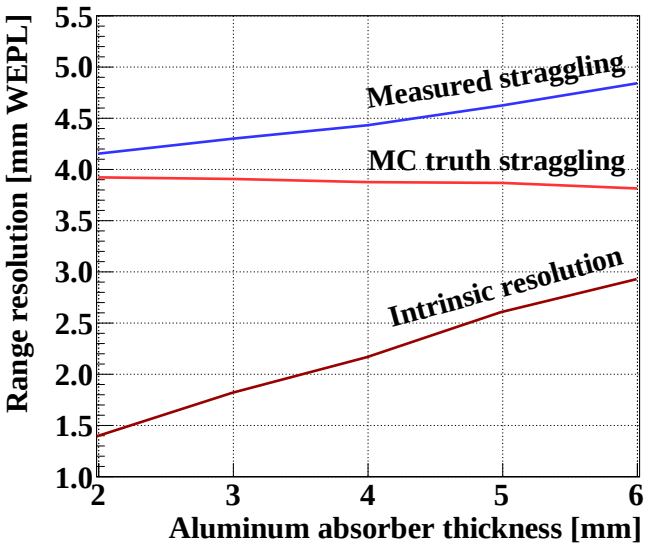

Figure 9: The range uncertainties of the proposed designs. Shown in the figure is the total uncertainty, the range straggling from the MC truth as well as the added uncertainty which is the quadratic difference between the two. See Table 2 for the number of required layers for the shown designs [13].

tracker layers due to its thermal properties. A design applying CF, the flexible PCB board and the ALPIDE chips has been suggested: its material budget is 120 µm aluminum, 160 µm polyimide, 100 µm silicon, 300 µm CF and 30 µm epoxy glue. The resulting radiation length [19] is $X_0 = 14$ cm.

We assume that the scattering in a single event taking place near the first sensor layer, and that the first sensor layer is positioned $L = 10$ cm after the patient as in Bopp *et al.* [14]. The degraded resolution due to scattering in the first two sensor layers is most precisely calculated by performing a full image reconstruction study, however an approximation is found by projecting σ_{MCS} onto the phantom—given as $L\sigma_{\text{MCS}}$ by Poludniowski *et al.* [16]. This lateral deflection should be kept as low as possible and below 1 mm.

The resulting value of σ_{MCS} is 7.1 mrad. Hence, the lateral deflection on the object is given by $L\sigma_{\text{MCS}} = 0.7$ mm. To keep this error within 1 mm, we need to apply a distance L of below 14 cm, a task that seems feasible when compared to other systems [6, 28].

7. DISCUSSION

The optimal design of the pixel-based range telescope must fulfill the following ambitions: High accuracy of the range determination; low uncertainty (standard deviation) of the range determination, limited by the inherent proton range straggling; high track reconstruction efficiency, *i.e.* the ability to disentangle and reconstruct all the protons in a single readout frame; and other constraints such as economy (number of layers), cooling and mechanical stability.

Based on these requirements and constraints, as well as on the results in Pettersen *et al.* [5], we find that the longitudinal size of the detector should be designed with aluminum energy absorption layers between the sensor layers, this layer should be 3.5 mm thick, corresponding to approx. 7.5 mm WET. With this thickness, around 41 layers are needed in order to fully contain the range of a 230 MeV proton beam within the detector, including a 3σ range straggling longitudinal extension. Using this geometry, the intrinsic range uncertainty is 2 mm WET, compared to the range straggling of 3.8 mm WET that is added to this number in quadrature. A systematic oscillating error is introduced to the range determination

accuracy due to the layer structure of the detector. By applying 3.5 mm thin aluminum absorbers, the oscillation is kept below 0.2 mm WET. Since this is a systematic uncertainty, it is not possible to reduce it by increasing the number of protons per projection.

The track reconstruction efficiency increases rapidly with decreasing absorber thickness, and from this perspective, the absorber thickness should be kept below 4 mm and as low as possible. At 200 protons in the pencil beam per readout, when using the 2 mm (4 mm) 6 mm aluminum absorber geometry the fraction of correctly reconstructed tracks is 93% (84%) 66%—a significant difference.

The first low-mass tracker layers enabling the calculation of the incoming proton trajectory have been proposed stabilized with a thin layer of carbon fiber. The total mass of the layers is 0.5% X_0, ensuring that the scattering angle of a proton in the energy range of interest is ~7 mrad. Poludniowski *et al.* [16] propose a limit of 1 mm on the uncertainty of this scattering angle projected onto the imaged object: this corresponds here keeping the distance between the imaged object and the tracker layers to $L < 14$ cm. This distance is also expected to have an effect on the performance of the track reconstruction—the more spread out the pencil beam is (increased distance), the easier it is to correctly reconstruct the tracks (less particle density).

In this study, several simplifications regarding the detector design has been made. The detector layers have been modeled using slabs of homogeneous materials. Structures in the sensor chips and electronics might introduce systematic errors in the range calculations. In addition, the final material budget of the sensor chips and electronics for a layer might deviate from the design assumed in this study (see Figure 1). However, the goal of this study has been to find the accuracy of the range calculations and evaluate the track reconstruction algorithms, in designs applying energy degrading absorbers of 2–6 mm aluminum—the added material budget is of a significantly higher amount than the eventual uncertainties in the implementation of the sensor chips and electronics.

8. CONCLUSION

In this study we have investigated the performance of different conceptual designs of a pixel-based range telescope using MC simulations together with the analysis framework developed for a proof-of-concept prototype investigated earlier [5].

The analysis was performed by combining tracking of individual protons and Bragg curve modeling of each protons energy loss. The detector is expected to have the capability of tracking 10–30 million protons per second, assuming realistic electronics- and design proposals. The range uncertainties are close to the range straggling limit, and any systematic errors in the range determination are kept below 0.3 mm WET throughout the detector. By considering the presented results, the optimal material choice for the energy-absorbing layers is 3.5 mm aluminum.

The proposed low-mass tracker layers are expected to introduce a positional uncertainty on the proton's position at the object exit in the order of 0.7 mm, below the limit of 1 mm from Poludniowski *et al.* [16].

The range accuracy improvement achieved by using absorbers of thicknesses 3 mm or less is negligible due to the inherent range straggling limit. Thicker absorbers, however, yield a systematic oscillating error in accuracy of the range determination, and at thicknesses of 5 mm and higher this effect will significantly degrade the accuracy.

In terms of the reconstruction efficiency, a thinner absorber improves the efficiency by a large amount. Hence, the thickness should not be significantly above 3 mm. When considering the overall system complexity, a 4 mm absorber requires fewer sensor layers (37 layers) compared to the 3 mm (corresponding to 47 layers) design, and thus the 4 mm, or an 3.5 mm design with 41 layers, could represent an optimal trade-off between efficiency/accuracy and construction constraints.

9. ACKNOWLEDGEMENTS

An earlier version of this text is included in the first author's PhD dissertation [13], a project which was supported by Helse Vest (Western Norway Regional Health Authority, Stavanger, Norway) grant [911933].

REFERENCES

[1] R. P. Johnson, Review of medical radiography and tomography with proton beams, Reports on Progress in Physics 81 (1) (2018) 016701. doi:10.1088/1361-6633/aa8b1d.

[2] H. Paganetti, Range uncertainties in proton therapy and the role of Monte Carlo simulations, Physics in Medicine and Biology 57 (11) (2012) R99–R117. doi:10.1088/0031-9155/57/11/R99.

[3] R. W. Schulte, S. N. Penfold, J. T. Tafas, K. E. Schubert, A maximum likelihood proton path formalism for application in proton computed tomography, Medical Physics 35 (11) (2008) 4849. doi:10.1118/1.2986139.

[4] C.-A. Collins-Fekete, L. Volz, S. K. N. Portillo, L. Beaulieu, J. Seco, A theoretical framework to predict the most likely ion path in particle imaging, Physics in Medicine and Biology 62 (5) (2017) 17771790. doi:10.1088/1361-6560/aa58ce.

[5] H. Pettersen, J. Alme, A. Biegun, A. van den Brink, M. Chaar, D. Fehlker, et al., Proton tracking in a high-granularity Digital Tracking Calorimeter for proton CT purposes, Nuclear Instruments and Methods in Physics Research Section A: Accelerators, Spectrometers, Detectors and Associated Equipment 860C (2017) 51–61. doi:10.1016/j.nima.2017.02.007.

[6] M. Esposito, C. Waltham, J. T. Taylor, S. Manger, B. Phoenix, T. Price, G. Poludniowski, S. Green, P. M. Evans, P. P. Allport, et al., Pravda: The first solid-state system for proton computed tomography, Physica Medica 55 (2018) 149154. doi:10.1016/j.ejmp.2018.10.020.

[7] S. Jan, G. Santin, D. Strul, S. Staelens, K. Assie, D. Autret, et al., GATE: a simulation toolkit for PET and SPECT, Physics in medicine and biology 49 (19) (2004) 4543. doi:10.1088/0031-9155/49/19/007.

[8] S. Agostinelli, J. Allison, K. Amako, J. Apostolakis, et al., Geant4-a simulation toolkit, Nuclear Instruments and Methods in Physics Research Section A: Accelerators, Spectrometers, Detectors and Associated Equipment 506 (3) (2003) 250–303. doi:10.1016/S0168-9002(03)01368-8.

[9] G. Aglieri Rinella, The ALPIDE pixel sensor chip for the upgrade of the ALICE Inner Tracking System, Nuclear Instruments and Methods in Physics Research Section A: Accelerators, Spectrometers, Detectors and Associated Equipment 845 (2016) 583–587. doi:10.1016/j.nima.2016.05.016.

[10] B. Abelev, J. Adam, D. Adamov, M. M. Aggarwal, G. Aglieri Rinella, M. Agnello, et al., Technical design report for the upgrade of the alice inner tracking system, Tech. Rep. CERN-LHCC-2013-024. ALICE-TDR-017, CERN (Nov 2013). doi:10.1088/0954-3899/41/8/087002. https://cds.cern.ch/record/1625842

[11] O. S. Grøttvik, Design of High-Speed Digital Readout System for Use in Proton Computed Tomography, MSc thesis, University of Bergen, Norway (Jun. 2017). http://bora.uib.no/handle/1956/16041

[12] L. Maczewski, Measurements and simulations of MAPS (Monolithic Active Pixel Sensors) response to charged particles - a study towards a vertex detector at the ILC, PhD, University of Warsaw, arXiv: 1005.3710 (May 2010).
http://arxiv.org/abs/1005.3710

[13] H. E. S. Pettersen, A Digital Tracking Calorimeter for Proton Computed Tomography, PhD thesis, University of Bergen, Norway (2018).
http://bora.uib.no/handle/1956/17757

[14] C. Bopp, R. Rescigno, M. Rousseau, D. Brasse, The impact of tracking system properties on the most likely path estimation in proton CT, Physics in Medicine and Biology 59 (23) (2014) N197–N210. doi:10.1088/0031-9155/59/23/N197.

[15] B. Rossi, K. Greisen, Cosmic-ray theory, Rev. Mod. Phys. 13 (1941) 240–309. doi:10.1103/RevModPhys.13.240.

[16] G. Poludniowski, N. M. Allinson, P. M. Evans, Proton radiography and tomography with application to proton therapy, The British Journal of Radiology 88 (1053) (2015) 20150134. doi:10.1259/bjr.20150134.

[17] M. Gómez Marzoa, Innovative low-mass cooling systems for the ALICE ITS upgrade detector at CERN, PhD, École Polytechnique Fédérale de Lausanne, Lausanne, CH (2016).

[18] The ALICE Collaboration, K. Aamodt, A. A. Quintana, R. Achenbach, S. Acounis, D. Adamov, et al., The ALICE experiment at the CERN LHC, Journal of Instrumentation 3 (08) (2008) S08002. doi:10.1088/1748-0221/3/08/S08002.

[19] Particle Data Group, Atomic and Nuclear Properties of Materials for more than 300 materials, accessed: 2018-01-12 (2015).
http://pdg.lbl.gov/2015/AtomicNuclearProperties/

[20] Y. Touloukian, R. Powell, C. Ho, P. Klemens, Thermophysical Properties of Matter - The TPRC Data Series. Volume 2. Thermal Conductivity - Nonmetallic Solids, Defense Technical Information Center, 1971.

[21] Goodfellow Inc., Polymethylmethacrylate material information, accessed: 2018-10-01 (2018).
http://www.goodfellow.com/E/Polymethylmethacrylate.html

[22] Mitsubishi Chemical, K13D2U datasheet, accessed: 2018-12-28 (2018).
https://www.900gpa.com/en/product/fiber/CF_00D7088B15?u=metric

[23] L. Grevillot, T. Frisson, N. Zahra, D. Bertrand, F. Stichelbaut, N. Freud, D. Sarrut, Optimization of GEANT4 settings for Proton Pencil Beam Scanning simulations using GATE, Nuclear Instruments and Methods in Physics Research Section B: Beam Interactions with Materials and Atoms 268 (20) (2010) 3295–3305. doi:10.1016/j.nimb.2010.07.011.

[24] M. J. Berger, J. Coursey, M. Zucker, J. Chang, ESTAR, PSTAR, and ASTAR: Computer Programs for Calculating Stopping-Power and Range tables for Electrons, Protons, and Helium Ions (2005).
http://physics.nist.gov/Star

[25] H. E. S. Pettersen, M. Chaar, I. Meric, O. H. Odland, J. R. Sølie, D. Röhrich, Accuracy of parameterized proton range models; a comparison, Radiation Physics and Chemistry 144C (2018) 295–297. doi:10.1016/j.radphyschem.2017.08.028.

[26] H. E. S. Pettersen, I. Meric, O. H. Odland, H. Shafiee, J. R. Slie, D. Röhrich, Proton Tracking Algorithm in a Pixel Based Range Telescope for Proton Computed Tomography, EPJ Web of Conferences, In Press.

[27] T. Bortfeld, An analytical approximation of the Bragg curve for therapeutic proton beams., Med Phys 24 (12) (1997) 2024–2033. doi:10.1118/1.598116.

[28] R. P. Johnson, V. Bashkirov, L. DeWitt, V. Giacometti, R. F. Hurley, P. P., T. E. Plautz, H. F. W. Sadrozinski, K. Schubert, R. Schulte, B. Schultze, A. Zatserklyaniy, A Fast Experimental Scanner for Proton CT: Technical Performance and First Experience With Phantom Scans, IEEE Transactions on Nuclear Science 63 (1) (2016) 52–60. doi:10.1109/TNS.2015.2491918.